Journal of Alloys and Compounds 486 (2009) 890–894

Contents lists available at ScienceDirect

Journal of Alloys and Compounds

journal homepage: www.elsevier.com/locate/jallcom

Optimized doping concentration of manganese in zinc sulfide nanoparticles for yellow-orange light emission

Jian Cao[a,b], Jinghai Yang[c,a,*], Yongjun Zhang[c], Lili Yang[c], Yaxin Wang[c], Maobin Wei[c], Yang Liu[c], Ming Gao[c], Xiaoyan Liu[c], Zhi Xie[d]

[a] Key Laboratory of Excited State Physics, Changchun Institute of Optics, Fine Mechanics and Physics, Chinese Academy of Sciences, 3888 Eastern Nan-Hu Road, Changchun 130033, PR China
[b] Graduate School of the Chinese Academy of Sciences, Beijing 100049, PR China
[c] The Institute of Condensed State Physics, Jilin Normal University, Siping 136000, PR China
[d] National Synchrotron Radiation Laboratory, University of Science and Technology of China, Hefei, Anhui 230029, PR China

ARTICLE INFO

Article history:
Received 19 April 2009
Received in revised form 16 July 2009
Accepted 16 July 2009
Available online 24 July 2009

Keywords:
Solvothermal
ZnS:Mn^{2+}
Photoluminescence

ABSTRACT

Nanocrystalline samples of ZnS and $Zn_{1-x}Mn_xS$ were synthesized by the solvothermal method without any surface-active agents and characterized by X-ray diffraction (XRD), transmission electron microscopy (TEM), high-resolution transmission electron microscopy (HRTEM), near-edge X-ray-absorption fine structure technique (XANES), photoluminescence (PL) and UV–vis. The results showed that the Mn^{2+} ions were substitutionally incorporated into the ZnS host and the size of the particles was decreased as the Mn doped-ratio increased. The yellow-orange emission from the Mn^{2+} $^4T_1$–$^6A_1$ transition was observed in the PL spectra, the peak intensity ratio of which to that of sulfur vacancies increased with the increase of the Mn^{2+} concentration, and showed a maximum when the concentration of Mn^{2+} was kept at 3%.

1. Introduction

Nanocrystals have been extensively investigated during the last decade due to their unique properties and application potential [1–4]. Luminescent semiconducting nanocrystals have attracted widespread attention for their practical applications: optical coatings, field effect transistors, photoconductors, optical sensors, photocatalysts, electroluminescent materials and other light-emitting materials [5–8]. Zinc sulfide, a typical II–VI compound semiconductor, with a direct band gap of 3.6 eV at room temperature and 40 meV as exciton binding energy, is a very good luminescent material used in displays, sensors and lasers [9–11]. Owing to the large band gap of ZnS, it can easily host different transition metal ions as luminescent centers. Among these transition metal ions doped nanostructures, Mn^{2+} doped ZnS exhibits its much more importance due to its attractive light-emitting properties for applications as efficient phosphors. According to Bhargava and Gallagher [12], when Mn^{2+} ions are incorporated into the ZnS lattice and substitute for the cation sites, the mixing between the sp electrons of host ZnS and the d electrons of Mn^{2+} occurs and makes the forbidden transition of $^4T_1$–$^6A_1$ partially allowed, resulting in the characteristic emission of Mn^{2+}.

In the past few years, a number of techniques have been employed to synthesize ZnS:Mn^{2+} nanoparticles, such as precipitation, sol–gel, solvothermal and thermal coevaporation at high temperature [13–19]. Among these methods, the solvothermal method requires a relatively low temperature, cheap precursors of low toxicity and makes easy the introduction of transition metal ions such as Mn^{2+} and Cu^{2+} into the ZnS lattice. To the best of our knowledge, few investigations have been reported on the optimized doping concentration of manganese in zinc sulfide nanoparticles via solvothermal method. Therefore, we are going to report a simple method for doping Mn^{2+} into ZnS nanoparticles and investigate the effect of Mn^{2+} concentration on the structure and optical properties of ZnS:Mn^{2+} nanoparticles. We would like to show that the solvothermal method is quite capable of addressing the doping issue in semiconductor nanostructures without any major modification.

2. Experimental

2.1. Preparation

ZnS:Mn^{2+} nanoparticles were prepared by the solvothermal technique. The analytical grade reagents of zinc acetate [$Zn(CH_3COO)_2{\cdot}6H_2O$], manganese acetate [$Mn(CH_3COO)_2{\cdot}4H_2O$] and thiourea ($NH_2CSNH_2$) were used as the initial materials. Appropriate amounts of [$Zn(CH_3COO)_2{\cdot}6H_2O$] and [$Mn(CH_3COO)_2{\cdot}4H_2O$] were dis-

* Corresponding author at: The Institute of Condensed State Physics, Jilin Normal University, Siping 136000, PR China. Tel.: +86 434 3290009; fax: +86 434 3294566.
E-mail address: jhyang1@jlnu.edu.cn (J. Yang).

0925-8388/$ – see front matter © 2009 Elsevier B.V. All rights reserved.
doi:10.1016/j.jallcom.2009.07.097

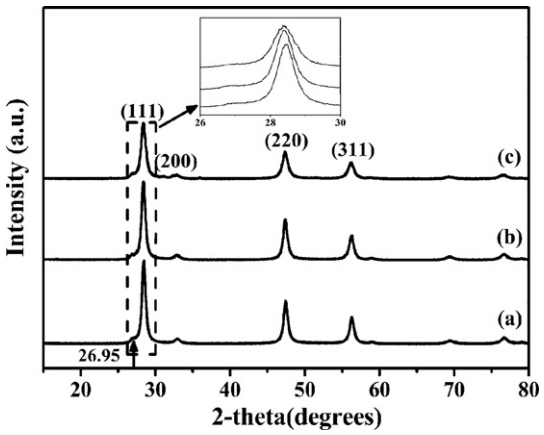

Fig. 1. XRD patterns of (a) ZnS, (b) ZnS:Mn^{2+} (3%), (c) ZnS:Mn^{2+} (11%) nanoparticles with the inset showing the XRD patterns between 26° and 30°.

solved in 16 mL ethanol first. After being stirred for 1 h, thiourea was put into the resulting solution (the ratio between the total amount of salt and sulfur was controlled to be 1:3). After being stirred for 2 h, the colloid solution was transferred into several 20-mL Teflon-lined autoclaves and kept at 180 °C for 12 h. After the reaction, the autoclaves were taken out and cooled to room temperature. The products were washed with ethanol and deionized water for several times and separated by centrifugation, and then dried at 80 °C for 1 h to get white powder.

2.2. Characterization

The products were analyzed by X-ray diffractometer (MACScience, MXP18, Japan) with Cu radiation, transmission electron microscopic (200 keV, JEM-2100HR, Japan), scanning electron microscopy (Hitachi, S-570), photoluminescence (PL) (Perkin-Elmer, LS55), UV (UV-3101PC) and near-edge X-ray-absorption fine structure technique (XANES). The specimens for the UV–vis absorption and transmittance measurements were dissolved in ethanol and placed in a 1 cm quartz cell, and ethanol served as the reference solvent. The specimens for the TEM measurements were prepared by depositing a drop of the dilute solution of the sample in 2-propanol on a carbon-coated copper grid and drying at room temperature. The EDAX microanalysis was performed at the SEM magnification. The samples for XRD, EDAX, PL and XANES measurements were solid powder. The Mn *K*-edge XANES measurements were performed at room temperature on beamline 1W1B at Beijing Synchrotron

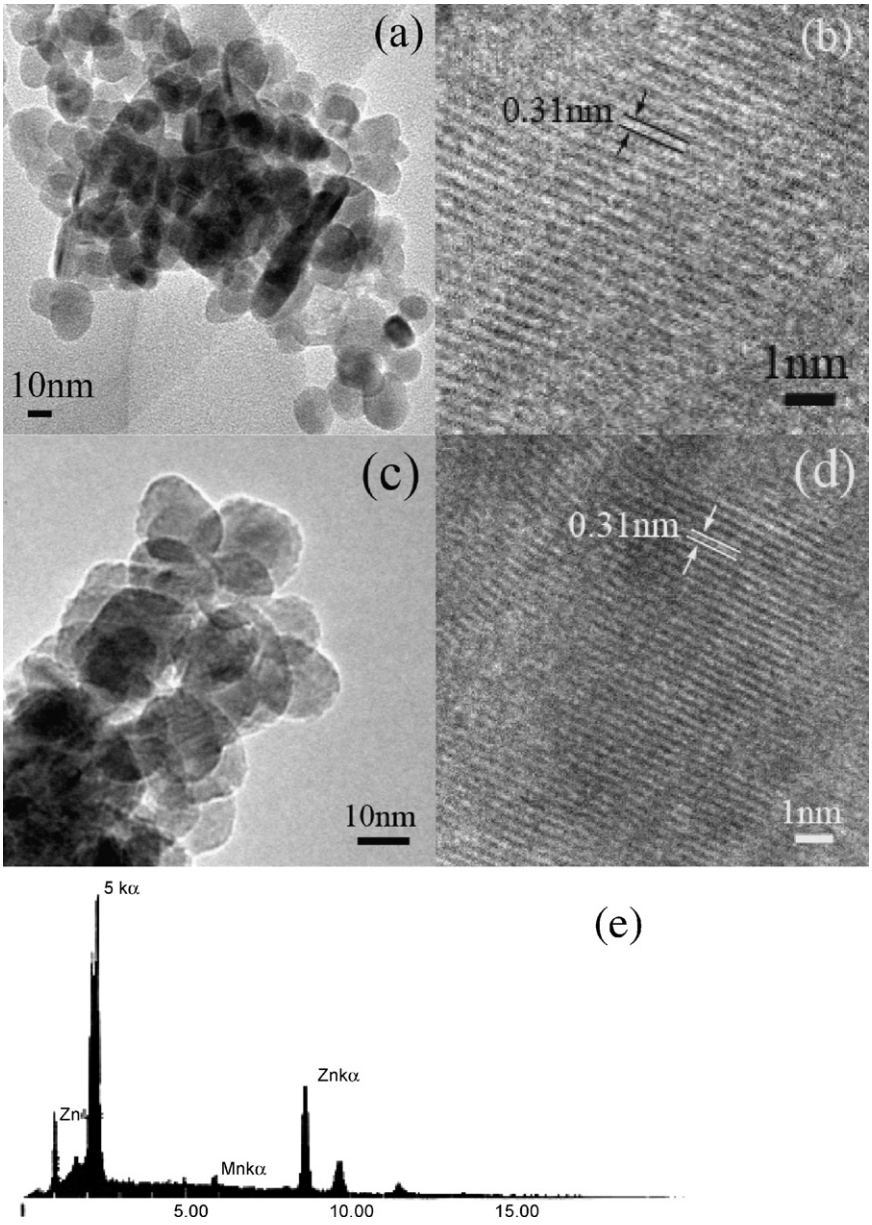

Fig. 2. (a) and (b) TEM and HRTEM images of ZnS nanoparticles, (c) and (d) TEM and HRTEM images of ZnS:Mn^{2+} (3%) nanoparticles, (e) EDAX image of ZnS:Mn^{2+} (3%) nanoparticles.

Radiation Facility, China. A double crystal Si (1 1 1) monochromator was used, and the signal was collected in fluorescence yield mode with a Lytle ion chamber detector. The data was collected in a mode of sample drain current under a vacuum better than 5×10^{-7} Torr.

3. Results and discussion

XRD patterns of the as-prepared $Zn_{1-x}Mn_xS$ ($x = 0$, 0.03, 0.11) nanoparticles are shown in Fig. 1. Three main peaks at 28.45° (1 1 1), 47.41° (2 2 0) and 56.29° (3 1 1) are observed, which are in good agreement with the standard card (JCPDS No. 05-0566). We can also observe a weak peak centered at 26.95°, which can be indexed as the (1 0 0) diffraction of wurtzite (the polymorph of the zinc blende). It indicates that the samples are mainly in zinc blende structure containing a small amount of ZnS in the hexagonal wurtzite structure. In addition, the shift to the low angle in the peak position of the XRD patterns indicates that the lattice constant of the $Zn_{1-x}Mn_xS$ nanoparticles increases with the Mn doped-ratio increased (see inset of Fig. 1). Since that the ionic radius of Mn^{2+} (0.83 nm) is 10% larger than that of Zn^{2+} (0.74 nm) [20]. According to the Bragg equation [21], the lattice constant of ZnS nanoparticles is calculated to be 5.409 Å, and a slight increase is obtained in the lattice constant of ZnS:Mn^{2+} nanoparticles which can be seen in Table 1. The average size estimated from the full width at half-maximum of the three main peaks using Debye–Scherrer formula [22] is about 16.1 nm (ZnS), 15.5 nm (3% Mn), 11.8 nm (11% Mn). So, the particle size is decreased as the Mn doped-ratio increased which is further demonstrated below by TEM and UV–vis studies. In addition, there is no extra diffraction peak from manganese ions, which indicates that the Mn^{2+} ions may be incorporated into the ZnS nanoparticles.

Fig. 2a–d shows the TEM and HRTEM images of ZnS and $Zn_{0.97}Mn_{0.03}S$ nanoparticles. It is observed that these nanoparticles are agglomerated with diameters of 12–18 nm for ZnS (Fig. 2a), 10–16 nm for $Zn_{0.97}Mn_{0.03}S$ (Fig. 2c), which is consistent with the value calculated from XRD. The HRTEM images (Fig. 2b and d) exhibit a clear lattice spacing of 0.31 nm, which matches with the distance of the (1 1 1) plane of the standard zinc blend ZnS [23]. The composition analysis by EDAX shown in Fig. 2e demonstrates that the sample contain Zn, S and Mn elements, and 1.9 at% Mn is detected for 3 at% Mn doped ZnS nanoparticles.

The optical properties of the samples are investigated from the absorption and transmittance measurements in the range of 280–700 nm. Fig. 3 shows the UV–vis absorption and transmittance spectra of $Zn_{1-x}Mn_xS$ ($x = 0$, 0.03, 0.11) nanoparticles. The results indicate that the samples have a direct band gap as expected. The optical band gap '*Eg*' can be calculated using the following relation:

$$\alpha = \frac{A(h\nu - Eg)^n}{h\nu}$$

where A is a constant and n is a constant, equal to 1/2 for direct band gap semiconductor. The estimated band gap from the plot of $(\alpha h\nu)^2$ versus $h\nu$ for $Zn_{1-x}Mn_xS$ ($x = 0$, 0.03, 0.11) nanoparticles can be seen in Fig. 4. The band gap '*Eg*' is determined by extrapolating the straight portion to the energy axis at $\alpha = 0$. It is found to be 3.51 eV ($x = 0$), 3.67 eV ($x = 0.03$) and 3.77 eV ($x = 0.11$), respectively. It indicates that the size of the particles is decreased as the Mn doped-ratio increased. The normalized Mn *K*-edge XANES spectrum for $Zn_{0.97}Mn_{0.03}S$ nanoparticles (Fig. 5) shows two characteristic peaks: A (6540 eV), B (6553 eV), which are in good agreement with the result of Soo et al. [24]. These near-edge features can be reproduced by the FEFF8.2 simulation [25] and the first-principles spin-polarized density functional theory calculation [26] when Mn ions occupy Zn sites in ZnS. These results have confirmed that the Mn ions are substitutionally incorporated into the ZnS lattice, and no Mn related secondary phase is formed. It should be noted that the preedge peak centered at 6540 eV is associated with the

Table 1
Dependence of the lattice constants of ZnS:Mn^{2+} on the Mn^{2+} concentration.

Mn concentration (%)	Lattice constant (calculated) Å
0	5.409
3	5.416
11	5.419

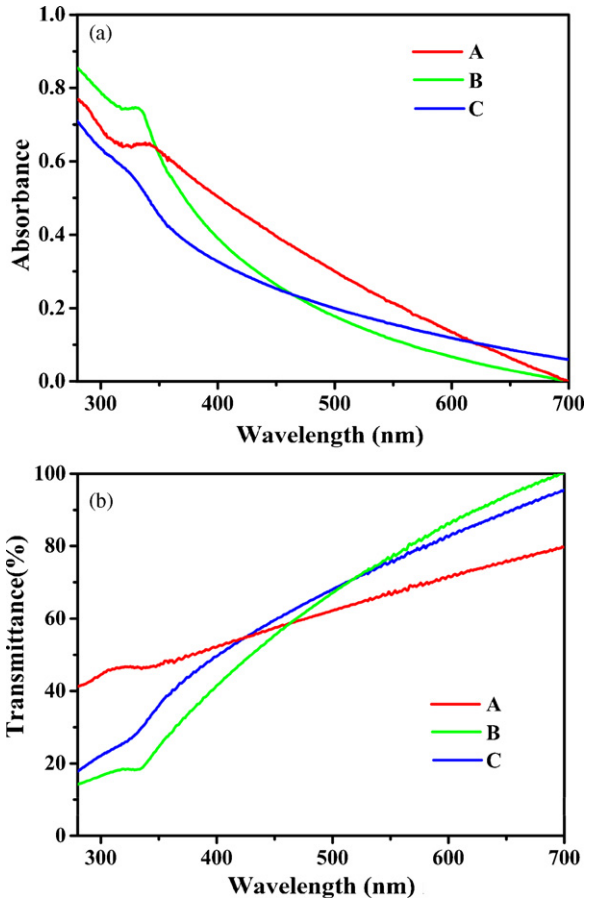

Fig. 3. The UV–vis (a) absorption and (b) transmittance spectra of (A) ZnS, (B) ZnS:Mn^{2+} (3%), (C) ZnS:Mn^{2+} (11%) nanoparticles.

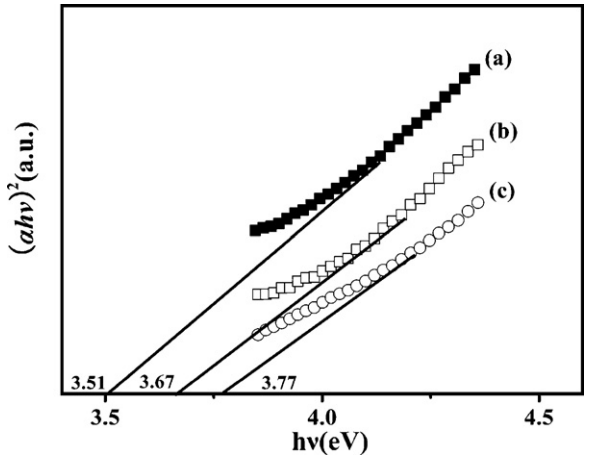

Fig. 4. The plot of $(\alpha h\nu)^2$ versus $h\nu$ of (a) ZnS, (b) ZnS:Mn^{2+} (3%), (c) ZnS:Mn^{2+} (11%) nanoparticles.

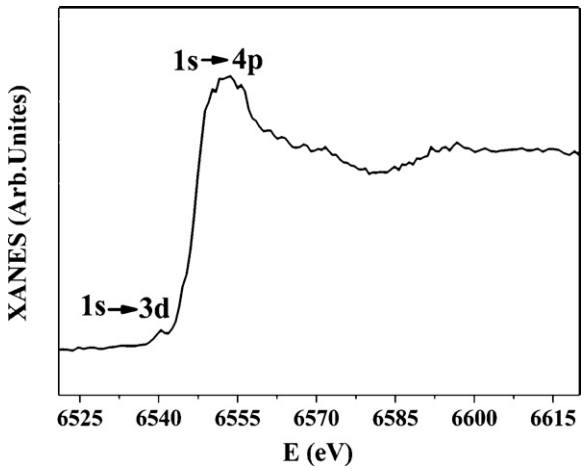

Fig. 5. Mn *K*-edge XANES spectrum of $Zn_{0.97}Mn_{0.03}S$ nanoparticles.

transitions from 1s states to the unfilled, narrow 3d states. It is well known that the Mn^{2+} ions have unfilled 3d electron shell and filled 3p electron shell. The 3d electrons do not normally participate in the absorption process unless there is a strong hybridization between sp hybrid orbital of ZnS and 3d orbital of Mn^{2+}.

Photoluminescence spectra for ZnS and $Zn_{1-x}Mn_xS$ ($x = 0.01$, 0.02, 0.03, 0.05, 0.11) nanoparticles can be seen in Fig. 6. The spectra were recorded at the excitation wavelength of 330 nm, 320 nm, 300 nm, with an emission filter at 430 nm in the 400–700 nm range. For all the samples, the blue-green emission ranging from 400 nm to 500 nm can be ascribed to the defect states in the ZnS nanoparticles. The peaks centered at 440 nm and 485 nm are from the sulfur vacancies and zinc vacancies emission, respectively [27–29]. Note that the peak position of this emission band shifts to the lower energy when different excitation wavelengths are employed (330 nm, 320 nm, 300 nm). It has been reported that the red shift is caused by the coupling action among the ZnS nanoparticles and the interaction between the ZnS nanoparticles and their surrounding environment [29]. For the samples doped with Mn^{2+}, the yellow-orange emission centered at ~590 nm can be observed besides the blue-green emission, which is associated with the $^4T_1$–$^6A_1$ transition within the 3d shell of Mn^{2+}. According to Bhargava and Gallagher [12], the yellow-orange emission is attributed to an efficient energy transfer from the ZnS host to Mn^{2+} ions facilitated by the mixed electronic states. When Mn^{2+} ions are incorporated into the ZnS lattice and substitute for the cation sites, the mixing between the s–p electrons of the host ZnS and the d electrons of Mn^{2+} occurs and makes the forbidden transition of $^4T_1$–$^6A_1$ partially allowed, resulting in the characteristic emission of Mn^{2+}, which is in coincidence with the XANES results.

Previously, Sooklal et al. [30] studied the effect of the location of Mn^{2+} on the photophysics of ZnS nanoparticles. They found that Mn^{2+} incorporation into the ZnS lattice lead to the orange emission while ZnS with surface-bound Mn^{2+} yielded the ultraviolet emission. As a comparison with our own results, it can be suggested that the Mn^{2+} ions are incorporated into the ZnS nanoparticles. To find the optimal doping concentration of Mn, the relative intensity ratio of the third PL peak (I_{Mn}) with respect to the first peak (I_{ZnS}) is plotted against Mn^{2+} concentration, which can be seen in Fig. 7. For different excitation wavelengths (330 nm, 320 nm, 300 nm), these spectra show the same variation: the relative peak intensities keep increasing until the Mn^{2+} concentration is up to 3% and then slightly decrease when the Mn^{2+} concentration continually increase to 11%. The results of the increase part indicate

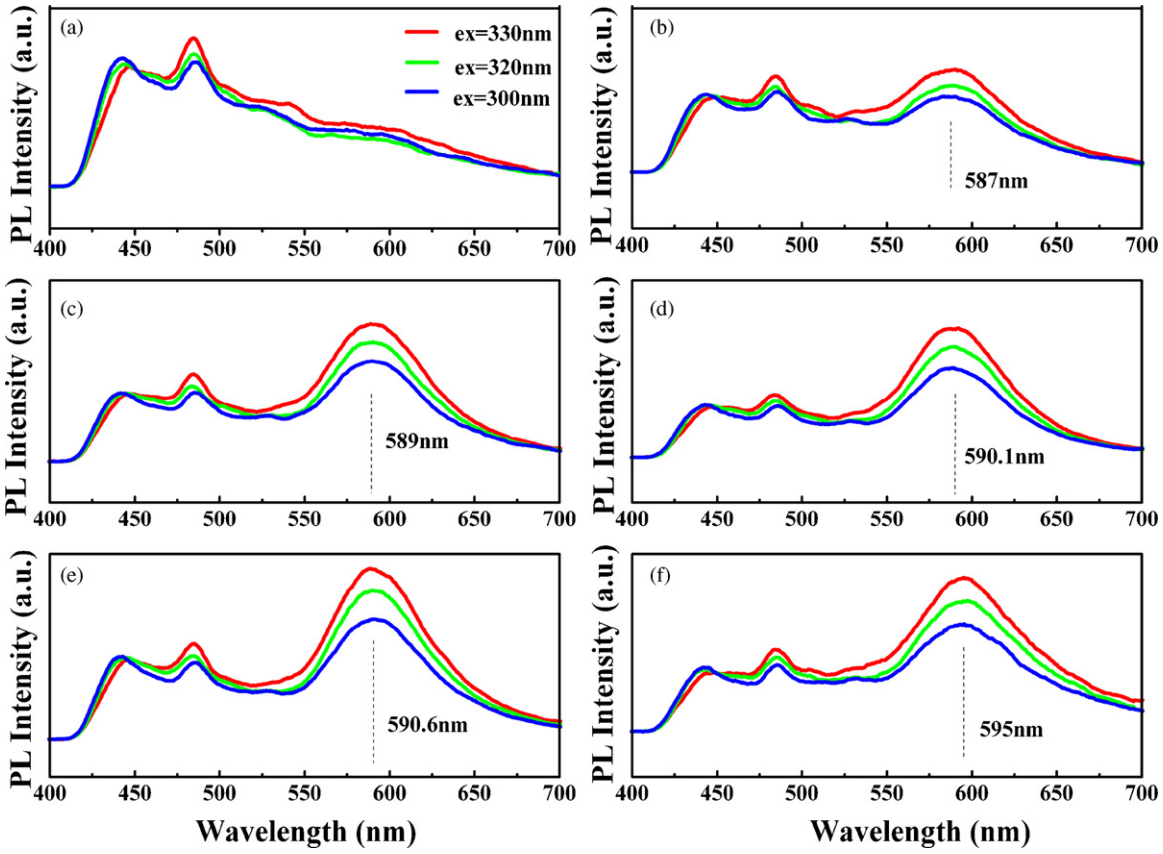

Fig. 6. The PL spectra of (a) ZnS, (b) ZnS:Mn^{2+} (1%), (c) ZnS:Mn^{2+} (2%), (d) ZnS:Mn^{2+} (3%), (e) ZnS:Mn^{2+} (5%), (f) ZnS:Mn^{2+} (11%) nanoparticles.

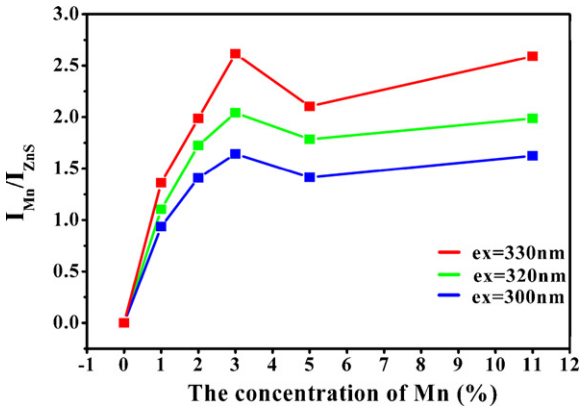

Fig. 7. Dependence of the relative peak intensity of the PL peak (I_{Mn}) with respect to the first peak (I_{ZnS}) on the Mn^{2+} concentration.

that the doped Mn^{2+} ions are the major luminescent component in ZnS nanoparticles, which have an optimal doping concentration of Mn at 3%. The slight decrease part may be caused by the Mn–Mn interaction [23].

In comparison with the emission spectra of $Zn_{1-x}Mn_xS$, a red shift about 8 nm of the yellow-orange emission is clearly seen in Fig. 6b and f, which have been observed by many groups [15,31–34]. Three mechanisms can be used to explain the red shift: first, it may be due to the high density of surface states or strong electron–phonon coupling effects [31,33,34]. In fact, the surface area per unit volume for nanoparticles is increased as the particle size decreased. So, it would bring more defects states on the surface as the Mn doped-ratio increased. Second, when the Mn^{2+} concentration in ZnS nanoparticles exceeds a critical limit, a MnS phase tends to form. Manganese, the emitting center, sits in an octahedral site in the MnS phase instead of a tetrahedral site. In this case, the energy level of the d orbital of Mn is affected by the stronger crystal field in octahedral coordination than in tetrahedral coordination. As a result, the energy difference between the $^4T_1$ state and the $^6A_1$ state decreases. Therefore, PL emission will shift from yellow to red [32,35,30]. The third explanation is based on the nonradiation energy transfer in Mn clusters, an exchange mechanism leads to the excited Mn^{2+} ion resonantly transferring its energy to its neighbors, until a red center is encountered [15,32]. The explanations mentioned above can enlighten us to clarify the underlying mechanism of the red shift orange emission for the further detailed work.

4. Conclusions

In conclusion, ZnS nanoparticles doped with various Mn^{2+} concentrations were successfully synthesized through the solvothermal technique. There was a slight decrease in the particle size for the samples as the Mn^{2+} content increased. The effect of Mn^{2+} concentration on the optical properties of ZnS:Mn^{2+} has been investigated. The peak intensity ratio of Mn^{2+} $^4T_1$–$^6A_1$ emission to sulfur vacancies emission increased as the Mn^{2+} content increased, and showed a maximum when the concentration of Mn^{2+} was kept at 3%, and a further increase of the Mn^{2+} concentration would lead to the decrease of the intensity ratio of the two peaks. A red shift about 8 nm of Mn^{2+} $^4T_1$–$^6A_1$ emission is observed by comparing ZnS:Mn^{2+} (1%) with ZnS:Mn^{2+}(11%).

Acknowledgments

This work was financially supported by the National Natural Science Foundation of China (Grant No. 60778040 and 60878039), National Programs for High Technology Research and Development of China (863) (Item No. 2009AA03E303), Program for the development of Science and Technology of Jilin province (Item No. 20082112), the Science and Technology bureau of Key Program for Ministry of Education (Item No. 207025) and Cooperation Program between NSRL and BSRF.

References

[1] V.L. Klimov, S.A. Lvanov, J. Nanda, Nature 447 (2007) 441.
[2] M. Bruchez Jr., M. Moronne, A. Paul Alivisatos, Science 281 (1998) 2013.
[3] X. Fang, Y. Bando, M. Liao, U.K. Gautam, C. Zhi, B. Dierre, B. Liu, Adv. Mater. 21 (2009) 2034.
[4] Y. He, H.-F. Wang, X.P. Yan, Chem. Eur. J. 15 (2009) 5436.
[5] Z. Wang, L. Daemen, Y. Zhao, C.S. Zha, Nat. Mater. 4 (2005) 922.
[6] A.A. Green, M.C. Hersam, Nano Lett. 8 (2008) 1417.
[7] L. Yin, Y. Bando, Nat. Mater. 4 (2005) 883.
[8] T. Toyama, T. Hama, D. Adachi, Nanotechnology 20 (2009) 055203.
[9] H.C. Ong, R.P.H. Chang, Appl. Phys. Lett. 79 (2001) 3612.
[10] Y.C. Fang, S.Y. Chu, H.C. Chen, J. Electrochem. Soc. 156 (2009) k55.
[11] S. Kar, S. Biswas, J. Phys. Chem. C 112 (2008) 11144.
[12] R.N. Bhargava, D. Gallagher, Phys. Rev. Lett. 72 (1994) 416.
[13] D.-R. Jung, D. Son, J. Kim, C. Kim, B. Park, Appl. Phys. Lett. 93 (2008) 163118.
[14] L. Yue, F. Zhang, J. Huang, L. Wang, J. Nanosci. Nanotechnol. 8 (2008) 1199.
[15] R. Maity, K.K. Chattopadhyay, Nanotechnology 15 (2004) 812.
[16] A.K. Keshari, A.C. Pandey, J. Appl. Phys. 105 (2009) 064315.
[17] C.-H. Lu, B. Bhattacharjee, S.-Y. Chen, J. Alloys Compd. 475 (2009) 116.
[18] S. Biswas, S. Kar, S. Chaudhuri, J. Phys. Chem. B 109 (2005) 17526.
[19] G. Hajisalem, M. Marandi, N. Taghavinia, Nanotechnology 20 (2009) 095706.
[20] X. Wang, J. Xu, H. Chen, J. Phys. Chem. C 112 (2008) 17581.
[21] Z.W. Quan, Z.L. Wang, P.P. Yang, J. Lin, J.Y. Fang, Inorg. Chem. 46 (2007) 1354.
[22] P. Vinotha Boorana Lakshmi, K. Sakthi Raj, K. Ramachandran, Cryst. Res. Technol. 44 (2009) 153.
[23] W.Q. Peng, S.C. Qu, G.W. Cong, Z.G. Wang, J. Cryst. Growth 282 (2005) 179.
[24] Y.L. Soo, Z.H. Ming, S.W. Huang, Y.H. Kao, Phys. Rev. B 50 (1994) 7602.
[25] A.L. Ankudinov, B. Ravel, J.J. Rehr, S.D. Conradson, Phys. Rev. B 58 (1998) 7565.
[26] M. Kunisu, F. Oba, H. Ikeno, I. Tanaka, T. Yamamoto, Appl. Phys. Lett. 86 (2005) 121902.
[27] M.V. Limaye, S. Gokhale, S.A. Acharya, S.K. Kulkarni, Nanotechnology 19 (2008) 415602.
[28] D. Dong, L. Lan, X. Zhang, H. Xu, An. Haiping, Chin. Phys. Lett. 24 (2007) 2661.
[29] Q. Wu, H. Cao, S. Zhang, X. Zhang, D. Rabinovich, Inorg. Chem. 45 (2006) 7316.
[30] K. Sooklal, B.S. Cullum, S.M. Angel, C.J. Murphy, J. Phys. Chem. 100 (1996) 4551.
[31] Z. Ren, H. Yang, L. Shen, S.D. Han, J. Mater. Sci: Mater. Electron. 19 (2008) 1.
[32] J. Ge, J. Wang, H. Zhang, Y. Li, Adv. Funct. Mater. 2 (2005) 303.
[33] N. Karara, S. Rajb, F. Singhc, J. Cryst. Growth 268 (2004) 585.
[34] N. Karar, F. Singh, B.R. Mehta, J. Appl. Phys. 95 (2004) 656.
[35] Z. Zhang, J. Wang, H. Yuan, Y. Gao, J. Phys. Chem. B 109 (2005) 18352.